High performance Fin-FET electrochemical sensor with high-k dielectric materials

Serena Rollo[a,b], Dipti Rani[a], Wouter Olthuis[b], César Pascual García[a,*]

[a] Nano-Enabled Medicine and Cosmetics group, Materials Research and Technology Department, Luxembourg Institute of Science and Technology (LIST), Belvaux, Luxembourg
[b] BIOS Lab on Chip Group, MESA + Institute for Nanotechnology, University of Twente, Enschede, theNetherland

ABSTRACT

In this work we combine a Fin Field Effect Transistor (Fin-FET) characterised by a high height to width aspect ratio with high-k dielectric materials to study the optimized design for chemical-FETs to provide higher transconductance (and thus a better signal to noise ratio), increased dynamic range and chemical stability. We used pH sensing to verify the design. We explored the sensitivity and linearity of the response of silicon dioxide, alumina and hafnium oxide as dielectric materials sensing pH, and compared their chemical stability in different acids. The high aspect ratio fin geometry of the sensor provides high currents, as well as a planar conduction channel more reliable than traditional silicon nanowires. The hafnium oxide Fin-FET configuration performed the best delivering the most linear response both for the output and transfer characteristics, providing a wider dynamic range. Hafnium oxide also showed the best chemical stability. Thus we believe that the developed high aspect ratio Fin-FETs/high-k dielectric system can offer the best compromise of performance of FET-based sensors.

1. Introduction

Bio-Field Effect Transistors (Bio-FETs) are FET based sensors combined with a biological recognition element able to sense biomolecules. They are an interesting alternative for label free detection of biomarkers in the fields of genomics [1–3] and proteomics [4–6] for applications in medical diagnostics, drug discovery and basic research, offering multiplexing capability, portability and miniaturisation, real-time analysis, selectivity, low cost. Despite these desirable features there is not yet a portable, low cost device in the market based on this technology. In fact there are challenges to overcome when scaling up from the laboratory to the industry level related to the reliability of the performance among devices, the functionalization with the bio-recognition element and the chemical stability of the surface [7–9], in particular for applications that require an extended contact of the sensor surface with the sample fluid. To improve the performance of Bio-FETs and chemical-FETs in general the original design of planar devices evolved into nano-sensors like nanowires [10], and new materials were introduced to increase the transduced signal and chemical stability of the interface [11–13]. Owing to the miniaturisation achieved by nanowires the sensitivity of label free sensing increased from μM to fM and the incubation time needed for heavy molecules to reach the equilibrium decreased from days to hours or minutes [14,15]. Nevertheless, the improved sensitivity of nano devices came at the cost of impacting negatively the signal to noise ratio and the variability of the current signal among devices [16,17]. Recently we proposed a Fin-FET design with a high aspect ratio of the height to width (> 10) in which the width of the sensor was comparable to that of nanowires but, due to the bigger height, it resulted in a planar conduction channel [18]. This change in the geometry improved the signal to noise ratio and the linearity of the output signal, and provided a higher surface area which is favourable for the reliability of the functionalisation as compared to nanowires. The device design provides a compromise to increase the total signal while providing a good response time for assays at low concentrations, for which the sensing is diffusion limited [19].

The dielectric interface of the FET in contact with the electrolyte is a key component of the sensor as it determines its chemical stability [20] as well as the transduction. It can be used as receptor for simple molecules or ions in solution such as protons [21,22] or as the support for the functionalisation of biorecognition layers that improve the selectivity of the sensor [23]. In the case where the interface is directly used to capture molecules, the surface chemical properties of the dielectric itself determine the surface potential that regulates the conductivity of the transistor across the source to drain channel. The

* Corresponding author.
  E-mail address: cesar.pascual@list.lu (C. Pascual García).

conduction is also affected by the dielectric constant (k) of the material that determines the capacitance effect between the sensor surface and the conduction channel. The fabrication of devices with silicon dioxide (SiO_2) as dielectric interface is convenient but it is not preferable since SiO_2 has low pH buffer capacity in comparison to other dielectric materials and it suffers from drift, hysteresis, leakage currents, and penetration of ions when in contact with the electrolyte for an extended period of time [24,25]. Other dielectrics such as aluminium oxide (Al_2O_3) [11,12,26], hafnium oxide (HfO_2)12,27] and tantalum pentoxide (Ta_2O_5) [28,29] can be used to improve the sensor properties, being more resistant to ion penetration and providing a higher dielectric constant that increases the transconductance further by increasing the capacitive effect in the semiconductor, even with physically thicker layers. Combining the design of a high aspect ratio Fin-FETs with high-k dielectrics can enhance their specific advantages, improving the superior linear response of the output current and increasing the sensitivity and signal to noise ratio by improving the transconductance responsible of the signal transduction. Materials with better chemical performance, meaning higher intrinsic buffer capacity, while also being more resistant to dissolution in both acidic and basic conditions, have the potential to provide reliability and stability to the device.

To measure the impact of the dielectric in FETs, the detection of the acidity of a solution in aqueous electrolytes (pH) has been used as a direct comparison of the performance among different oxides [30,31]. The response of the dielectric towards pH can be described using the combined Gouy-Chapman-Stern and Site-Binding (GCS-SB) models, where the GCS model describes the electrical double layer that forms at the oxide interface, and the SB model describes the grade of ionization (protonation or deprotonation) of the surface chemical groups of the dielectric barrier [32]. Using both models it is possible to derive the relationship between the bulk pH and the potential at the oxide surface (Ψ_0), characterised by the oxide sensitivity $\Delta\Psi_0/\Delta pH$ which determines the chemical response of the material. Silicon oxide shows pH sensitivities of 20–40 mV/pH depending on the quality of the grown layer, and a nonlinear response in a wider pH range due to its low intrinsic buffer capacity [33–36]. Al_2O_3, HfO_2 and Ta_2O_5 have shown sensitivities equal or higher than 55 mV/pH, and improved linearity in a wide pH range [11,28,30,37]. HfO_2 and Ta_2O_5 have similar values of the dielectric constant but the conduction band offset with silicon is 0.34 and 1.4 respectively for the two materials [38]. This makes HfO_2 a better choice than Ta_2O_5, which also suffer of light induced drift [39]. An ultimate design of a FET sensor has to combine the sensor geometry with the effect of the dielectric material on the transduction and of the surface properties on the chemical performance (sensitivity and stability).

In this work we combine a p-doped high aspect ratio Fin-FET design with different dielectrics as thermally grown SiO_2 and atomic layer deposited Al_2O_3 and HfO_2 on a thin SiO_2 adhesion layer, which were the oxides available in our facilities. ALD deposited Al_2O_3 has been widely used as sensing dielectric layer in electrochemical FET sensors so we could compare our grown material with the existing literature. HfO_2 is a higher-k material than alumina, with better chemical stability, which promises the best performance. We have studied the pH sensitivity in terms of variations of Ψ_0, which we relate to the intrinsic properties of the material (dissociation constants of the surface active groups and surface density of the surface reactive sites). We also compare the effects of transducing the variations of Ψ_0 within two similar Fin-FET devices with SiO_2 and HfO_2, respectively. Using a Nernst-Poisson model [18] we calculate the effective dielectric constant of the stack SiO_2/HfO_2. Finally, we test the stability of the three oxides comparing a controlled citric acid buffer with natural citrus juices. We proved that while Al_2O_3 represents an improvement to SiO_2, HfO_2 provides the best chemical stability in time and overall enhances the transduction properties of the Fin-FETs. Owing to the combination of the high aspect ratio of the sensors configuration with the high-k and chemically stable HfO_2

we report the highest performance of this electrochemical sensor.

2. Materials and methods

2.1. Silicon Fin-FETs fabrication

We fabricated silicon Fin-FETs by anisotropic wet etching of p-doped silicon on insulator (SOI) substrates with a 2 ± 0.1 and $3 \pm 0.1\,\mu m$ thick silicon device layer ($< 110 >$ oriented) with resistivity of 0.115 Ω·cm (equivalent doping 10^{17} /cm^3) and a 1 μm thick buried SiO_2 procured from Ultrasil Corporation. The substrates were diced in chips of 1×1 cm^2 before starting the fabrication of the Fin-FETs. Briefly, we used Maskless photolithograpy (MLA 150 Heidelberg Instruments) and e-beam lithography (FEI Helios electron microscope) on the negative resist ma-N 2403 to pattern lines with widths ranging from 400 to 700 nm on a thermally grown thin SiO_2, oriented along the direction parallel to the primary flat of the substrate in order to get the desired shape after wet etching. The Fin-FET shape originates from the different rates at which the $< 110 >$ and the $< 111 >$ planes are etched. The device lateral walls lay on the $< 111 >$ planes. The etching along the vertical direction ($< 110 >$ plane) is about 10 times faster than along the $< 111 >$ planes. Knowing the plane dependent etching rates [40] and device layer thickness of Si, lithography mask was designed with defined line widths to have final wire width on the chips. The connection between the lines and the contact pads was achieved through approaching pads with a triangular footprint designed at the angles of $\approx 54.7°$ and 35.3° with respect to the primary flat to provide a smooth profile between the channel and the pads after etching. This pattern was then transferred to the previously thermally grown oxide by Reactive Ion Etching (RIE) through a CF$_4$ process of 15 min at a pressure of 75 mTorr and power of 25 W. The samples were then treated with HF to remove the excess of oxide outside the lithographed area and to obtain a smooth surface. The anisotropic etching was achieved with a 25% wt Tetramethylammonium hydroxide, 8.5%vol of Isopropanol water solution lasting for ≈ 23 and ≈ 30 min for the complete etching of the 2 and 3 μm thick substrates, respectively. After a 1 min dip in HF to remove the SiO_2 mask, samples were ready for the deposition of the gate oxide stacks. We used 20 nm of thermally grown SiO_2, and 10 nm atomic layer deposited (ALD) Al_2O_3 and HfO_2 with 7 nm of SiO_2 thermally grown as interlayer between the silicon and the ALD grown oxides to have the pH sensitive layers. First we grow the thin layer of SiO_2 to ensure a smoother interface and improve adhesion, also reducing pin-holes and leakages. Then we equalized the deposited thickness of Al_2O_3 and HfO_2 to approximately the same value as SiO_2. Indeed, all of them can be considered of similar values within the error margins of our thickness measurement equipment (3 nm).

Fig. 1(a) schematically shows the fabrication steps. Fig. 1(b) and (c) show Scanning Electron Microscope (SEM) pictures of a representative device with top and tilted views respectively. The high aspect ratio Fin-FET channel is shadowed in blue between the source and drain contact pads which are shadowed in red. The ohmic contacts and the leads necessary for the integration into a plastic circuit board (PCB) were defined by optical lithography on regions of the devices shadowed in red part. The ohmic contacts were a Ti/Al/Au stack (2/160/5 nm) e-beam evaporated, while the leads were Au 150 nm. Another lithography step on an epoxy (SU8) allowed to open windows on the Fin-FET region while protecting the contacts. After wire bonding to the PCBs dipstick, the samples were protected with a medical grade epoxy glue (Loctite EA M-31CL, Henkel). The final devices had a length of 14 μm at the middle of the Fin-FET and width ranging from 150 to 400 nm. Each chip contained eleven Fin-FETs. Table 1 summarizes the characteristics of thickness of the deposited oxide (t_{ox}), average width (w) of the devices on the same chip with the same oxide, and height (h) of the fabricated devices.
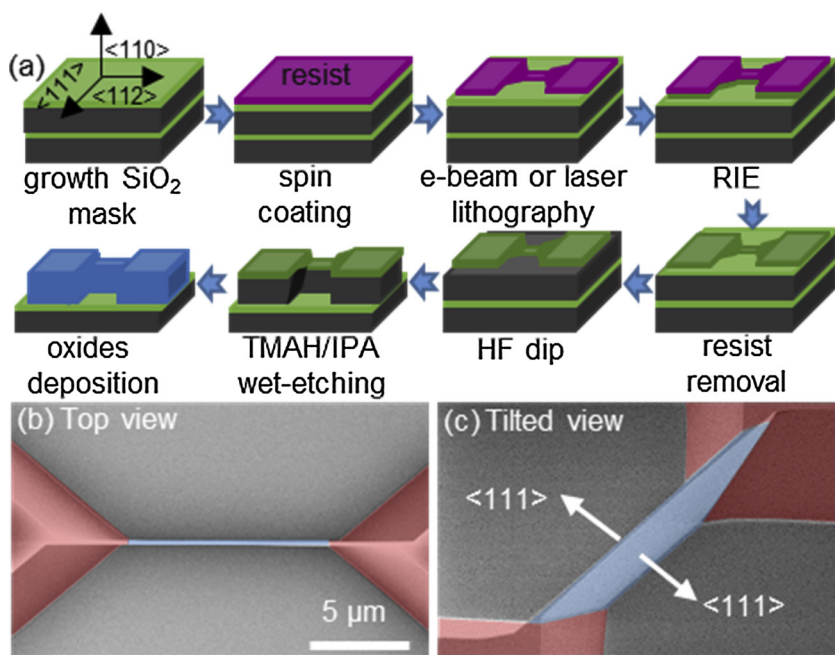
Fig. 1. (a) Schematic representation of the fabrication process of Fin-FETs on SOI substrates based on laser or e-beam lithography on a negative resist, and wet etching in a TMAH/IPA wet etching solution. Silicon is represented in dark grey while silicon oxide is represented in green. The resist is depicted in purple and the final oxide as sensing layer in blue. The crystallographic directions on the SOI substrate are represented by black arrows. (b) and (c) Top and tilted SEM pictures respectively of one representative Fin-FET device after fabrication. The silicon body of the Fin-FET device and the contacts are shadowed in blue and red, respectively. The crystallographic direction of the lateral walls of the device is represented by white arrows in (c).

Table 1

Characteristics of thickness of the deposited oxide (t_{ox}), and width (w) and height (h) of the fabricated devices.

Device oxide	t_{ox} (nm)	w (nm)	h (μm)
SiO_2	20	≈170	2
Al_2O_3	10	≈400	2
HfO_2	10	≈200	3

2.2. pH sensitivity characterization

Experiments of pH sensitivity were carried out in buffer solutions with pH from 3 to 11 in step of 1. The buffers were prepared by mixing a solution of KH_2PO_4, citric and boric acids at 0.1 M all, with a KNO_3 0.1 M solution in equal volume proportion, for a final pH of 2.5. More basic pH buffer solutions were obtained by addition of a 0.1 M solution of KOH. All the solutions were prepared using Milli-Q water as solvent. With this procedure, the total ionic strength remained constant at 0.1 M. For the electrochemical characterization the chips were immersed into the buffer solutions with a calomel reference electrode (BioLogic R-XR300) for biasing the electrolyte and a commercial pH meter (Sentron SI600) to check the pH throughout the measurements. We used a Keithley 2614HB DC source meter to apply the voltage between the source and drain contacts and to the reference electrode and a multiplexer Keithley 3706A System Switch/Multimeter connected to a switching box to characterize the devices in sequence.

2.3. Measurements of acidity in citrus juices

First, we prepared a solution of citric acid 0.01 M by dissolving 0.48 g in 250 mL of Milli-Q water. The resulting solution had an acidic pH of 3 measured with a commercial pH meter. The lemon and orange juices were obtained from freshly squeezed fruits and filtering the pulp. Their pH was also measured with the pH meter, resulting in pH 2.7 and 4.1 for the lemon and orange juice respectively. For the measurements of citric acid we used the same set-up described in the paragraph above.

3. Results and discussion

3.1. Surface sensitivity of Fin-FETs with SiO_2, Al_2O_3, HfO_2

In order to determine the surface sensitivity of the grown oxides, we measured the transfer characteristics, source drain current (I_{ds}) vs. reference electrode voltage (V_{ref}), at constant source drain voltage (V_{ds}). The pH sensitivity ($\Delta V_{ref}/\Delta pH$) was evaluated from the shift of the transfer curves at a constant current with different buffers pH values. The variations of the reference electrode voltage (ΔV_{ref}) compensate (and correspond to) the changes in the surface potential ($\Delta \Psi_0$) induced by the different proton concentrations. The choice of V_{ds} followed from a preliminary characterization performed at neutral pH and $V_{ref} = 0$ V. For this characterization we measured the output current I_{ds} vs. V_{ds} from all devices. At higher V_{ds} values we observed the pinching off of the carrier density in the channel by the deviation of the current characteristics from the linear behaviour. We restricted the study to the linear range of I_{ds} versus V_{ds} in order to be able to explain the variation of the conductance of the device with the ohmic contribution of the conducting channel cross section, and its dimensions. To this objective, for the characterization we used a V_{ds} of 0.1 V for the narrower devices (like the ones reported for SiO_2 and HfO_2), and 0.5 V for the wider ones (like the ones reported for Al_2O_3), while V_{ref} was swept in a range between -0.6 and 0.6 V in all cases. The transfer characteristics were acquired in a pH range between 3 and 11 in steps of 1 by immersing the samples into the buffer solutions. Multiple Fin-FETs on three different chips having the three oxides as pH sensitive layers were characterized with the same procedure. Fig. 2(a)–(c) show the transfer characteristics of three representative devices from each type family of dielectrics. At each oxide is attributed a colour and different shades are used to indicate the 1 unit pH change between the measurements, according to the coloured scales as shown in Fig. 2(a)–(c). The width of the tested devices (w) is also specified. In each case we observed a shifting of the transfer characteristics toward more positive V_{ref} while moving from acidic to basic buffers. This is because the majority carriers in the semiconductor channel are holes affected by Ψ_0. When the pH increases there are less protons interacting with the oxide surface, thus lower Ψ_0 compared to more acidic conditions. Therefore higher V_{ref} is required to compensate the electrostatic potential at the oxide liquid interface to maintain a constant current flowing through the channel. Fig. 2(d)–(f)
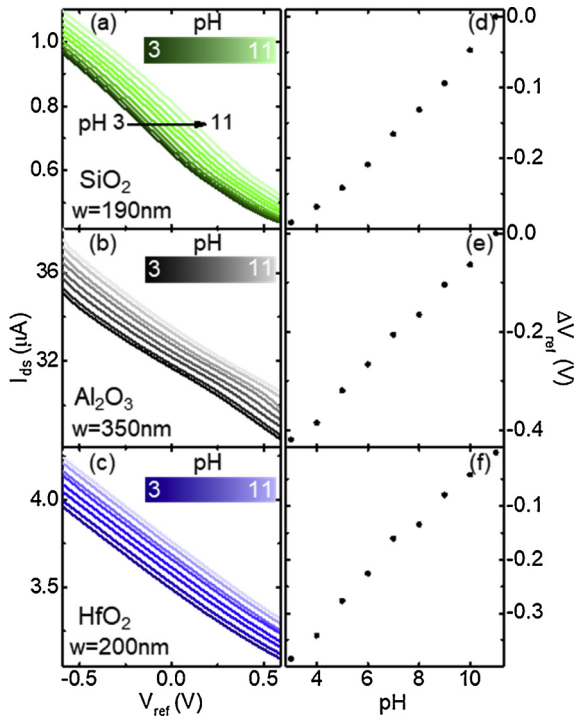
Fig. 2. (a)–(c) Examples of transfer characteristics I_{ds} vs V_{ref} at fixed V_{ds} for three representative devices with the three different oxides represented with coloured scales. The curves were measured in buffers at pH 3 to 11 in steps of 1, represented by different shades of the same colour attributed to each oxide. The width of the devices is referred as w. (d) to (f) V_{ref} vs pH measured from the curves in (a) to (c) from which the sensitivity of the oxide was evaluated as shifts of V_{ref} at each pH to maintain a constant current.

show the shift of V_{ref} with pH in the curves in Fig. 2(a)–(c) derived as the V_{ref} necessary to keep the value of I_{ds} at $V_{ref} = 0$ V constant from the value at pH 11, which corresponds to the variations of Ψ_0 due to the different proton concentrations. The relation between the surface potential and the pH is derived by combining the electrostatic interactions at the dielectric surface and the distribution of ions inside the electrolyte starting from the oxide surface, which was found earlier [30]:

$$\frac{\Delta\Psi_0}{\Delta pH_B} = -2.303\frac{k_B T}{q}\alpha \tag{1}$$

Where pH_B, k_B, T and q represent the pH in the bulk electrolyte, the Boltzmann constant, the absolute temperature and the elementary charge, respectively. α is a sensitivity parameters with a value varying between 0 and 1 depending on intrinsic properties of the oxide. For $\alpha = 1$ the sensor has a so called Nernstian sensitivity of 59.2 mV/pH at 298 K. We obtained an estimation of the sensitivity of the different oxides from the linear fit of the curves like the ones showed in Fig. 2(d)–(f) acquired from all the devices, obtaining the average value of the sensitivity and the standard deviation for each type of oxide. We found that the response of the dielectrics to different proton concentrations, which experimentally translates into a shift of the transfer characteristics at different pH values, were qualitatively similar among Fin-FETs with the same oxide. Al_2O_3 provided the best performance in terms of sensitivity with 54.2 ± 1.9 mV/pH, while the one for HfO_2 was 49.8 ± 0.6 mV/pH. For both oxides the experimental results are in agreement with other values of sensitivities reported in literature [11,12,26,27]. While Al_2O_3 and HfO_2 have an approximately linear response in the pH range considered, SiO_2 has a lower sensitivity in acidic conditions compared to basics due to the lower intrinsic buffer capacity of the oxide surface at low pH where the groups at the surface interacting with the protons in electrolyte are close to saturation and are not able to buffer the changes of proton concentration. In the pH

range between 6 and 11, where silicon oxide has the highest sensitivity, we estimated a value of 42.1 ± 0.5 mV/pH. Close to saturation (*i.e.* at the point of zero charge of the oxide surface, pH_{pzc}), at pH lower than 6, we estimated a sensitivity of 30.2 ± 1.1 mV/pH. These values are also in agreement with other values reported in literature [31–34].

The origin of the different pH sensitivities among the different oxides can be explained in terms of the acidic and basic dissociation constants (K_a and K_b, respectively) of the reactive groups (hydroxyls $-$ OH bound to Si, Al and Hf able to exchange protons) from each oxide surface, and the surface density of surface reactive sites (N_s). The combination of the Site Binding model which describes the reactivity of the hydroxyl groups, with the Gouy-Chapman-Stern model which describes the formation of an electrical double layer at the oxide/electrolyte interface, gives an expression for the sensitivity parameter α in Eq. (1) containing the differential capacitance C_{diff} and the intrinsic buffer capacity β_{int}.

$$\alpha = \frac{1}{\frac{2.303kTC_{diff}}{q^2\beta_{int}} + 1} \tag{2}$$

The differential capacitance depends on the electrolyte (solvent dielectric constant and ionic strength), while β_{int} depends on K_a, K_b, and N_s and is linked to the ability of the oxide to buffer small changes of surface charge [32]. Higher values of β_{int} are related to more reactive surfaces, thus improved sensitivities. From the experimental pH sensitivities, we evaluated α using Eq. (1). We also estimated C_{diff} using the estimation of C_{diff} presented in literature by Van Hal et al. that modelled C_{diff} as the series capacitance of the Stern capacitance C_{St} (the contribution of the layer of charges in closest contact with the oxide) and the diffuse layer capacitance C_{DL} (from Gouy and Chapman) [32]. C_{St} has been theoretically calculated for different ionic strengths of the electrolyte [41], and we used the same value considered by Van Hal et al. of 0.8 F/m^2. For the estimation of C_{DL} it is assumed that the total charge in the diffuse layer (σ_{DL}) is equal to the charge at the oxide surface (σ_0), which yields the expression for C_{DL} derived by Van Hal et al. [32]:

$$\sigma_{DL} = -(8kT\varepsilon_0\varepsilon_w n^0)^{1/2}sinh\left(\frac{zq\Psi_0}{2kT}\right) = -C_{DL}\Psi_0 = -\sigma_0 \tag{3}$$

Where ε_0, ε_w and n^0 are the vacuum and water relative permittivities, and the number concentration of each ion of the electrolyte, respectively. Using Eq. (3) we calculated the experimental C_{diff} for an electrolyte with a 0.1 M ionic strength as the one we used in our experiments, and combining it with the experimental sensitivity in Eq. (2) we calculated the experimental buffer capacity β_{calc}. We compared β_{calc} with the intrinsic buffer capacity obtained using literature values of the acidic and basic dissociation constants of the surface reactive groups (K_a, K_b), and surface density of surface reactive sites (N_s) [30,32,42], according to the expression for β_{int} given by Van Hal et al., as reported in S.I.. We calculated β_{calc} values of 0.6×10^{18}, 1.5×10^{18} and 1.7×10^{18} groups/m^2, for SiO_2, Al_2O_3 and HfO_2 respectively, compared to the values obtained by using literature data β_{lit} of 0.9×10^{18}, 3.7×10^{18} and 2.8×10^{18} groups/m^2, respectively. The results are summarized in Table 2.

In each case we noticed that the values of intrinsic buffer capacity calculated from our experimental data are lower than the ones obtained

Table 2

Values of the intrinsic buffer capacities for the three different oxides calculated from the results of pH sensitivity (β_{calc}) and obtained using values of K_a, K_b and N_s taken from literature for the three oxides (β_{lit}).

Device oxide	β_{calc} (groups/m^2)	β_{lit} (groups/m^2)
SiO_2	0.6×10^{18}	0.9×10^{18}
Al_2O_3	1.5×10^{18}	3.7×10^{18}
HfO_2	1.7×10^{18}	2.8×10^{18}

using data available in literature. The difference may be attributed to the different way the oxides are grown, the presence of impurities on the oxide surface, and defects coming from the deposition step that affect the total number of reactive sites.

3.2. Relevance of Fin-FETs integration with high-k dielectrics

Higher k dielectrics yield improvements to the sensor. Fin-FETs with high aspect ratio show more linear and higher transconductance $\Delta I_{ds}/\Delta pH$, respect to SiNWs18. We expect that higher k dielectrics will further improve the output characteristics of these devices. We compared the conductance of two Fin-FETs devices with the two oxides having the most different dielectric constants, meaning the ones with 20 nm thermally grown silicon oxide and the one with 10 nm of hafnium oxide grown on a 7 nm silicon dioxide interface layer, for a total thickness of about 17 nm. Both devices had approximately the same base width and length (190 nm and 14 μm, respectively), and heights of 2.16 ± 0.1 and 2.90 ± 0.1 μm for the SiO_2 and HfO_2, respectively (measured by profilometry).

The output characteristics I_{ds} vs V_{ds} were explored in a pH range from 3 to 11 with $V_{ref} = 0$ V. We choose this value of V_{ref} since at neutral pH I_{ds} was linear in a range of V_{ref} between -200 and 200 mV, which is the variation of surface potential expected in the considered pH range. Thus I_{ds} can be described with the ohmic contribution of the non-depleted region with a Nernst-Poisson model. I_{ds} was acquired by sweeping V_{ds} between -100 and 100 mV. I_{ds} had a linear behaviour in that range, as shown in Fig. 3(a) for the devices with SiO_2 and HfO_2 using colour scales for pH between 3 and 11 with steps 1. From the data in Fig. 3(a) we estimated the conductance (G) as the slope of the linear fittings. In Fig. 3(b) we report the conductance of the two Fin-FETs with the different sensing oxides normalized by the cross section of the device, to take into account for the difference in height and allow a comparison. The experimental data are represented as green triangles and blue dots for the devices with SiO_2 and HfO_2, respectively. The conductance increases towards more basic pH values in both cases as I_{ds} depends on the surface potential Ψ_0 which depends on the proton concentration, as already explained. The variation of the conductance we obtained was of 522 ± 12 mS/pH and of 912 ± 19 mS/pH per unit area for the SiO_2 and the HfO_2 devices respectively. The effect of enhanced variation of the conductance in the device with HfO_2 is due to the contribution from the higher intrinsic sensitivity of the material $\Delta\Psi_0/\Delta pH$, and to the higher dielectric constant, which increases the transconductance in the device. The higher linear response of the HfO_2 pH surface sensitivity is transferred to the output response. The higher sensitivity offered by HfO_2 through the whole acidity range combined

with the high aspect ratio fin geometry of the sensor channel offers better performances in a wider dynamic range.

We estimated the dielectric constant of the HfO_2 layer (ε_{HfO2}) using a Nernst-Poisson model to fit the experimental data (blue line in Fig. 3(b)) combined with the experimental sensitivity parameter α retrieved from the $\Delta V_{ref}/\Delta pH$. The model is based on Eq. (1) to describe the dependence of Ψ_0 with pH, that modulates the Poisson distribution of charges determining the depleted region that lastly controls the output current (a more detailed description can be found in our previous article [18]). The effective dielectric constant ε_{eff} of the SiO_2/HfO_2 stack was modelled with two capacitors in series from each oxide layer with known thicknesses ($t_{SiO2} = 7$ nm and $t_{HfO2} = 10$ nm measured during the growth in a dummy sample with ellipsometry):

$$\varepsilon_{eff} = \frac{(t_{SiO2} + t_{HfO2})\varepsilon_{SiO2}\varepsilon_{HfO2}}{t_{SiO2}\varepsilon_{HfO2} + t_{HfO2}\varepsilon_{SiO2}} \tag{4}$$

Considering the dielectric constant for SiO_2 $\varepsilon_{SiO2} = 3.9$ we obtained ε_{eff} of 7.4, and thus from Eq. (4) $\varepsilon_{HfO2} \approx 20$, which is in agreement with other values in literature for ALD deposited HfO_2 [37,43]. The calculation of the effective dielectric constant for the SiO_2/Al_2O_3 stack can be found in S.I.. The integration of high aspect ratio Fin-FETs with high-k materials provided the best performance in the output currents of the sensors for linearity and sensitivity.

3.3. Stability of the oxides in different acidic media

To study the stability over time of the different oxides in contact with fluids, we used the Fin-FETs with the three different interfaces to sense the acidity of squeezed lemon and orange juices where the main component responsible of the acidity is citric acid (7%, and 4–5%, concentration for lemon and orange juice, respectively). We compared the behaviour of the devices in citric juices with a 0.01 M citric acid buffer (pH 3) monitoring the fluctuations of the output current while moving the sensors from one liquid to another. We tested a family of devices for each oxide with a common external reference electrode moving the devices alternatively between water and the other acid solutions every 15 min and waiting five minutes before starting the next measurement to allow the stabilization of the sensor. To avoid cross contamination the sensors were rinsed with deionized water and blow dried with nitrogen in between each exchange of solutions. Fig. 4 shows the output currents as average values (using dots) for each cycle of the same devices shown in Fig. 2. The water, citric acid buffer, lemon and orange juices solutions are represented with blue, red, yellow and orange colours, respectively. The real-time output current plot over the 15 min duration of each interval can be found in S.I.. The insets shows pictures of the juices liquid samples used in the experiments. HfO_2 showed a very reproducible behaviour throughout the measurements. The current returned to approximately the same values depending on the pH of the solution with a drift < 10 nA (5% of the measured range) along three hours of measuring time. This was not the case for Al_2O_3 and SiO_2. Specifically the current in the device with Al_2O_3 showed an abrupt change of about 40 nA (> 60%) after 1 h followed by an stabilisation. Then the device behaved similarly to the SiO_2 one, which in three hours had a drift of 12 nA (15%). We attribute the abrupt change in the Al_2O_3 to the corrosion by citric acid which provokes the detachment of material especially in the pH range 3–6 as reported in literature [44]. After the Al_2O_3 layer was totally corroded the SiO_2 beneath was exposed stabilizing the device. In the transfer characteristics recorded after the experiment we noticed a decrease of the pH sensitivity in line with values reported for SiO_2 (transfer characteristics reported in S.I.), which support our hypothesis. Energy Dispersive X-Ray (EDX) spectroscopy performed on two samples with the same Al_2O_3/SiO_2 bilayer before and after exposure to the same citric acid solution used during the experiment revealed that the signal from Al disappears in the treated sample, further confirming our hypothesis (details in S.I.).
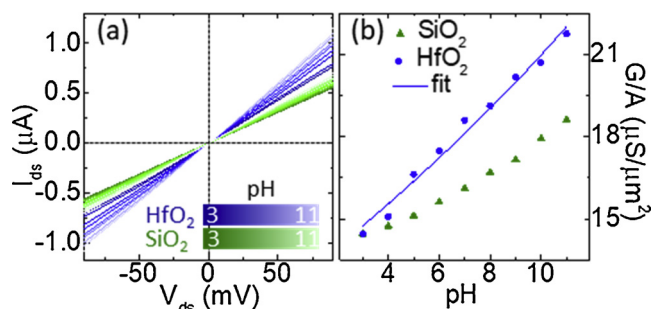

Fig. 3. (a) Output characteristics I_{ds} vs V_{ds} at fixed $V_{ref} = 0$ V for the SiO_2 and HfO_2 Fin-FETs respectively. The curves at different pH are coloured according to the scales in the inset. (b) Normalized conductance vs pH for the Fin-FETs having approximately the same width, with SiO_2 and HfO_2 as pH sensitive layers, calculated from the curves in Fig. 3 (a). The fitting of the experimental data with the Nernst-Poisson model used to estimate the dielectric constant of the deposited HfO_2 is represented as a blue line. (For interpretation of the references to colour in this figure legend, the reader is referred to the web version of this article).
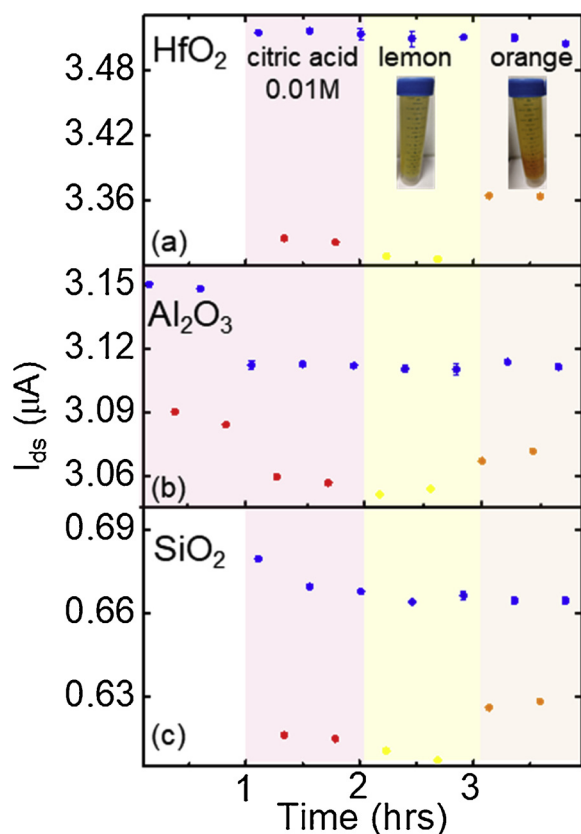
Fig. 4. (a)–(c) Output current I_{ds} vs time from three Fin-FETs devices with the three different oxides in different media which are represented in different colours. The dots represent the average current measured in 15 min, after which the samples were moved into a different solution. Pictures of the citrus juices used in the experiments are shown as an inset.

In the SiO_2 device the drift during the first hour is attributed to the intrinsic drifting normally observed in silicon oxide [24,45]. SiO_2 suffers issues of ions reactions and incorporation when in contact with electrolyte for an extended period of time which affects the oxide stability until an equilibrium is reached between the reactive groups at the oxide surface and ions in the solution, and the stability restored [24]. As discussed before, we obtained higher total average sensitivity for the HfO_2 Fin-FETs with a $\Delta R/R = 6.9\%$ (R refers to resistance of the device) between pH 7 and 2.8, compared to that of the SiO_2 FinFETs of $\Delta R/R = 5.9\%$ in the same range (after normalization to the cross section to take into account for the different heights).

4. Conclusions

In this work we investigated the surface sensitivity of different dielectric materials and the way they influence the transconductance in high aspect ratio Fin-FET chemical sensors. The chemical affinity of the different hydroxyl groups at the surface of the dielectrics provides the surface sensitivity of the material, which was tested by acidity measurements in a pH range from 3 to 11. We obtained surface sensitivities of 54.2 ± 1.9 mV/pH, 49.8 ± 0.6 and 37.5 ± 1.3 mV/pH for Al_2O_3, HfO_2 and SiO_2 respectively. While Al_2O_3 and HfO_2 had an approximately linear variation of the surface potential throughout the range investigated (pH 3–11), SiO_2 showed a lower sensitivity in acidic conditions attributed to the saturation of the reactive groups on the surface at low pH, next to the pH_{PZC}. We evaluated the experimental intrinsic buffer capacity (β_{int}) of the three oxides observing the poorer sensitivity of SiO_2 among the three oxides. We also investigated the effect of SiO_2 and HfO_2 on the transconductance of the Fin-FETs, and observed an almost doubled response for the HfO_2 which we attribute to the

enhanced surface sensitivity of the material as well as to the higher dielectric constant. This high aspect ratio Fin-FET/HfO_2 dielectric combination allows to increase the linearity of the output current with the concentration of the analyte and thus the dynamic range of the devices.

We investigated the stability of the three oxides when exposed to liquids for a long period of time by monitoring the fluctuations of the output currents of the three Fin-FETs families of oxides. We measured the acidity of different liquids other than ideal buffer solutions, such as citrus juices, where the acidity is mainly provided by the citric acid. In the device with HfO_2 the output current was stable, coming back at the same value after each change of the media. Along the three hours of the experiments we measured a drift of less than 5% of the measured range. For the device covered with Al_2O_3 we observed an abrupt change of more than 60% of the measured range after one hour, which we attributed to the corrosion of the material by the citric acid. The device with SiO_2 showed a drift of 15% of the measured range in the first hour, attributed to reactions of ions at the surface and ion incorporation, while the stability was restored after one hour.

In conclusion combining the Fin-FET geometry which intrinsically benefits an improved linearity in the transduction due to the 2D depletion along the width of the device, with high-k materials providing higher transconductance and chemical stability, improves the FET/dielectric material system offering higher performances of sensitivity and linearity of the response to provide wider dynamic ranges, and long term stability in liquid environment. These properties are all desirable features for biosensing applications and FET based biosensors development.

CRediT authorship contribution statement

Serena Rollo: Conceptualization, Methodology, Validation, Investigation, Data curation, Formal analysis, Writing - original draft, Writing - review & editing. **Dipti Rani:** Investigation, Writing - review & editing. **Wouter Olthuis:** Writing - review & editing. **César Pascual García:** Conceptualization, Funding acquisition, Project administration, Resources, Supervision, Methodology, Validation, Investigation, Writing - review & editing.

Declaration of Competing Interest

There are no conflicts to declare.

Appendix A. Supplementary data

Supplementary material related to this article can be found, in the online version, at doi:https://doi.org/10.1016/j.snb.2019.127215.

References

[1] Y.-C. Suy, W.-E. Hsu, C.-T. Lin, Review—field-effect transistor biosensing: devices and clinical applications, ECS J. Solid State Sci. Technol. 7 (7) (2018) Q3196–Q3207.
[2] Q. Li, N. Lu, L. Wang, C. Fan, Advances in nanowire transistor-based biosensors, Small Methods 2 (2018) 1700263.
[3] H-Y Park et al., M-DNA/transition metal dichalcogenide hybrid structure based Bio-FET sensor with ultrahigh sensitivity, Scientific Reports, 6:35733, DOI: 10:.1038/

srep35733.

[4] R. Ahmad, T. Mahmoudi, M.-S. Ahn, Y.-B. Hanh, Recent advances in nanowires-based Field-Effect Transistors for biological sensor applications, Biosens. Bioelectron. 100 (2018) 312–325.

[5] B. Ibarlucea, et al., Gating hysteresis as an indicator for silicon nanowire FET bio-sensors, Appl. Sci. 8 (2018) 950.

[6] I. Sarangadharan, S.-H. Huang, W.-C. Kuo, P.-H. Chen, Y.-L. Wang, Rapid detection of NT-proBNP from whole blood using FET based biosensors for homecare, Sens. Actuators B Chem. 282 (2019) 209–215.

[7] G.A. Urban, Micro- and nanobiosensors—state of the art and trends, Measurements Science and Technology 20 (2009) 012001.

[8] M.J. Schöning, A. Poghossian, Bio FEDs (Field-Effect Devices): state-of-the-art and new directions, Electroanalysis 18 (19–20) (2006) 1893–1900.

[9] C. Siontorou, F.A. Batzias, V.A. Tsakiri, Knowledge-based approach to online fault diagnosis of FET biosensors, IEEE Trans. Instrumentation and Measurements 59 (9) (2010) 2345–2364.

[10] M. Schwartz, T.C. Nguyen, X.T. Vu, P. Wagner, R. Thoelen, S. Ingebrandt, Impedimetric sensing of DNA with silicon nanowire transistors as alternative transducer principle, Phys. Status Solidi 215 (2018) 1700740.

[11] S. Chen, J. Bomer, E.T. Carlen, A. van der Berg, Al$_2$O$_3$/Silicon nanoISFET with near ideal Nernstian response, Nano Lett. 11 (2011) 2334–2341.

[12] K. Bedner, et al., pH response of silicon nanowire sensors: impact of nanowire width and gate oxide, Sens. Mater. 25 (8) (2013) 567–576.

[13] K. Malsagova, et al., Micro-Raman spectroscopy for monitoring of deposition quality of high-k stack protective layer onto nanowire FET chips for highly sensitive miRNA detection, Biosensors 8 (2018), https://doi.org/10.3390/bios8030072.

[14] J. Hahm, C.M. Lieber, Direct ultrasensitive detection of DNA and DNA sequence variations using nanowire nanosensors, Nano Lett. 4 (1) (2004) 51–54.

[15] K.S. Kim, H.-S. Lee, J.-A. Yang, M.-H. Jo, K. Hahn, The fabrication, characterization and application of aptamer-functionalized Si-nanowire FET biosensors, Nanotechnology 20 (23) (2008), https://doi.org/10.1088/0957-4484/20/23/235501.

[16] S. Vitusevich, I. Zadorozhnyi, Noise spectroscopy of nanowire structures: fundamental limits and application aspects, Semicond. Sci. Technol. 32 (2017) 043002.

[17] T.W. Wu, A. Alharbi, K.-D. You, K. Kisslinger, E. Stach, D. Shahrjedi, Experimental study of the detection limit in dual-gate biosensors using ultrathin silicon transistors, ACS Nano 11 (2017) 7142–7147.

[18] S. Rollo, D. Rani, R. Leturcq, W. Olthuis, C. Pascual García, High aspect ratio Fin-Ion Sensitive Field Effect Transistor: compromises toward better electrochemical bio-sensing, Nano Lett. (2019), https://doi.org/10.1021/acs.nanolett.8b04988.

[19] A. Alam, P.R. Nair, Performance limits of nanobiosensors, Appl. Phys. Lett. 88 (2006) 233120.

[20] P.D. van der Wal, D. Briand, G. Mondin, S. Jenny, S. Jeanneret, C. Milon, H. Roussel, C. Dubourdieu, N.F. De Rooij, High-k dielectrics for use as ISFET gate oxides, IEEE Sens. 24 (2004), https://doi.org/10.1109/ICSENS.2004.1426257.

[21] Y.-H. Chang, Y.-S. Lu, Y.-L. Hong, S. Gwo, J.A. Yeh, Highly sensitive pH sensing using an Indium Nitride Ion-Sensitive Field-Effect Transistor, IEEE Sens. J. 11 (5) (2011) 1157–1161.

[22] J. Artigas, A. Beltran, C. Jimenez, A. Baldi, R. Mas, C. Dominguez, J. Alonso, Application of ion sensitive field effect transistor based sensors to soil analysis, Comput. Electron. Agric. 31 (2001) 281–293.

[23] N. Chartuprayoon, M. Zhang, W. Bosze, Y.-H. Choa, One-dimensional nanos-tructures based bio-detection, Biosens. Bioelectron. 63 (2015) 432–443.

[24] I. Park, Z. Li, A.P. Pisano, R.S. Williams, Top-down fabricated silicon nanowire sensors for real-time chemical detection, Nanotechnology 21 (2010) 015501.

[25] S. Kum, D.W. Kwon, S. Kim, R. Lee, T.-H. Kim, H.-S. Mo, D.H. Kim, B.-G. Park, Analysis of current drift on p-channel pH-sensitive SiNW ISFET by capacitance measurement, Curr. Appl. Phys. 18 (2018) 568–574.

[26] J.-C. Chou, C.-Y. Weng, Sensitivity and hysteresis effect in Al2O3 gate pH-ISFET, Mater. Chem. Phys. 71 (2) (2001) 120–124.

[27] C.-S. Lai, T.-F. Lu, C.-M. Yang, Thickness effects on pH response of HfO$_2$ sensing dielectric improved by rapid thermal annealing, J. Appl. Phys. 45 (2006) 3807–3810.

[28] J.-W. Kang, W.-J. Cho, Improved pH sensitivity and reliability for extended gate Field-Effect Transistor sensors using high-k sensing membranes, J. Nanosci. Nanotechnol. 19 (2019) 1425–1431.

[29] T. Akiyama, Y. Ujihira, Y. Okabe, T. Sugano, E. Niji, Ion-Sensitive Field-Effect Transistors with inorganic gate oxide for pH sensing, IEEE Trans. Electron Devices (12) (1982) 1936–1941 ED. 29.

[30] A. Tarasov, et al., Understanding the electrolyte background for biochemical sensing with Ion-Sensitive Field-Effect Transistors, ACS Nano 6 (10) (2012) 9291–9298.

[31] P.V. Bobrov, Y.A. Tarantov, S. Krause, W. Moritz, Chemical sensitivity of an ISFET with Ta$_2$O$_5$ membrane in strong acid and alkaline solutions, Sens. Actuators B Chem. 3 (1) (1991) 75–81.

[32] R.E.G. Van Hal, J.C.T. Eijkel, P. Bergveld, A general model to describe the elec-trostatic at electrolyte oxide interfaces, Adv. Colloid Interfaces Sci. 68 (1996) 31–62.

[33] D. Rani, V. Pachauri, A. Mueller, X.T. Vu, T.C. Nguyen, S. Ingebrandt, On the use of scalable nanoISFET arrays of silicon with highly reproducible sensor performance for biosensor applications, ACS Omega 1 (2016) 84–92.

[34] S. Chen, J. Bomer, W. van der Wiel, E.T. Carlen, A. van der Berg, Top-down fab-rication of sub-30 nm monocrystalline silicon nanowires using conventional mi-crofabrication, ACS Nano 3 (11) (2009) 3485–3492.

[35] Y. Cui, Q. Wei, H. Park, C.M. Lieber, Nanowire nanosensors for highly sensitive and selective detection of biological and chemical species, Science 293 (5533) (2001) 1289–1292.

[36] S. Kim, et al., Silicon nanowire Ion Sensitive Field Effect Transistor with integrated Ag/AgCl electrode: pH sensing and noise characteristics, Analyst 136 (2011) 5012–5016.

[37] B.R. Dorvel, B. Reddy, J. Go, C.D. Guevara, E. Salm, M.A. Alam, R. Bashir, Silicon nanowires with high-k hafnium oxide dielectrics for sensitive detection of small nucleic acid oligomers, ACS Nano 6 (7) (2012) 6150–6164.

[38] S. Rigante, High-k Dielectric FinFETs on Si-bulk for Ionic and Biological Sensing Integrated Circuits, EPFL, 2014 Thesis No.6134.

[39] I. Yoshitaka, Long-term drift mechanism of Ta$_2$O$_5$ gate pH-ISFETs, Sens. Actuators B Chem. 64 (1-3) (2000) 152–155.

[40] S. Rollo, D. Rani, W. Olthuis, C. Pascual García, Single step fabrication of silicon resistors on SOI substrate used as thermistors, Sci. Rep. 9 (1) (2019), https://doi.org/10.1038/s41598-019-38753-x.

[41] X. Liu, F. Hu, W. Ding, R. Tian, R. Li, H. Li, A how-to approach for estimation of surface/Stern potentials considering ionic size and polarization, Analysts 140 (2015) 7217–7224.

[42] T. Akiyama, Y. Ujihira, Y. Okabe, T. Sugano, E. Niki, Ion-Sensitive Field-Effect Transistors with inorganic gate oxide for pH sensing, IEEE Trans. Electron Devices 29 (12) (1982) 1936–1941.

[43] S. Rigante, et al., Sensing with advanced computing technology: fin Field-Effect Transistors with high-k gate stack on bulk silicon, ACS Nano 9 (5) (2015) 4872–4881.

[44] M. Šeruga, D. Hasenay, Electrochemical and surface properties of aluminium in citric acid solutions, Appl. Electrochem 31 (2001) 961–967.

[45] T.-E. Bae, H.-J. Jang, J.-H. Yang, W.-J. Cho, High performance of silicon nanowire-based biosensors using a high-k stacked sensing thin film, ACS Appl. Mater. Interfaces 5 (2013) 5214–5218.

Serena Rollo is currently a Ph.D student at the Luxembourg Institute of Science and Technology working at the FNR Attract funded project NanoPH coordinated by Dr. Cesar Pascual Garcia, in co-supervision agreement with Prof. Dr. W. Olthuis from the University of Twente. She is working on the development of silicon field-effect transistors based electrochemical sensors for ion/biosensing applications. She obtained her Master and Bachelor science degrees in Materials Science and Engineering from the University of Bari, Italy.

Dipti Rani is currently working as a postdoctoral researcher in Luxembourg Institute of Science and Technology in FNR attract funded project NanoPH coordinated by Dr.Cesar Pascual Garcia. She received her Ph.D from Justus Liebig University Giessen, Germany, under the supervision of Prof. Martin Eickhoff and Prof. Sven Ingebrandt. Her Ph.D work was focussed on realization of silicon nanowire ion sensitive field-effect transistors for bio-chemical sensing applications. She obtained her Masters in Nanoscience and Nanotechnology from Joseph Fourier University, France, and her Bachelors in Physics (Honours) from Delhi University, India. Her current research interest encompasses na-nosensors development for bio-chemical applications.

Wouter Olthuis received his MSc. degree in electrical engineering from the University of Twente, Enschede, the Netherlands and then joined the Center for MicroElectronics, Enschede (CME) doing research on inorganic electric materials for subminiature silicon microphones. He received the PhD degree from the Biomedical Engineering Division of the Faculty of Electrical Engineering, University of Twente, in 1990. The subject of his dissertation was the use of iridium oxide in ISFET-based coulometric sensor-actuator devices. Since 1991 he has been working as an Assistant Professor in the Laboratory of Biosensors, part of the MESA$^+$ Research Institute of the University of Twente. Currently, he is Associate Professor in the BIOS Lab-on-Chip group of the MESA$^+$ Institute of Nanotechnology and is responsible for the theme Electrochemical sensors and Sensor systems. He has (co-)authored over 190 papers (h = 40) and 7 patents. From 2006 until 2011 he has also been the Director of the Educational Programme of Electrical Engineering at the Faculty of Electrical Engineering, Mathematics and Computer Science at the University of Twente. In 2011, he was appointed as officer on education in the executive committee of the IEEE Benelux section.

César Pascual García is lead research scientist at the Luxembourg Institute of Science and Technology, where he conducts the activities of electrochemical bio-sensors. He graduated in Physics at the *Universidad Autonoma de Madrid* (Spain), and obtained his Ph.D at the *Scuola Normale Superiore di Pisa* (Italy), studying the correlations of few electrons in quantum dots. He continued researching in the field of superconducting phenomena of metal heterojunctions at *NEST laboratories* in Pisa (Italy) before becoming Scientific Officer of the *European Commission* to serving at the *Institute for Health and Consumer Protection* in the group of Nano-Bio-Sciences. In 2014 he left to his current institute to lead an Attract project funded by the FNR to develop biopolymer microarrays driven by electrochemical synthesis. His current interests gravitate around sensors for personalised medicines and point of care devices.